# Low vaporization enthalpy of modified chitosan hydrogel for high performance solar evaporator

Patsaya Anukunwithaya[a,b], Nanxue Liu[a], Siqi Liu[a], Eknarin Thanayupong[b], Lili Zhou[a], Nuttaporn Pimpha[b], Jiakang Min[c], Wannee Chinsirikul[b], Warintorn Thitsartarn[d], J. Justin Koh[d*], and Chaobin He[a,d*]

[a]Department of Materials Science and Engineering, National University of Singapore, 9 Engineering Drive 1, Singapore 117575, Republic of Singapore.

[b]National Nanotechnology Center, National Science and Technology Development Agency, Thailand Science Park, Phahonyothin Road, Khlong Nueng, Khlong Luang, Pathum Thani, 12120, Thailand.

[c]Department of Chemistry, National University of Singapore, 3 Science Drive 3, Singapore 117543, Republic of Singapore.

[d]Institute of Materials Research and Engineering (IMRE), Agency for Science, Technology and Research (A*STAR), 2 Fusionopolis Way, Innovis #08-03, Singapore 138634, Republic of Singapore.

[*]Corresponding authors at:
Department of Materials Science and Engineering, National University of Singapore, 9 Engineering Drive 1, Singapore 117575, Singapore.
Institute of Materials Research and Engineering (IMRE), Agency for Science, Technology and Research (A*STAR), 2 Fusionopolis Way, Innovis #08-03, Singapore 138634, Republic of Singapore.
E-mail address: justin_koh@imre.a-star.edu.sg (J. Justin Koh), msehc@nus.edu.sg (Chaobin He)

**ABSTRACT**

The high vaporization enthalpy of water attributed to the strong hydrogen bonds between water molecules is limiting the performance of solar evaporators. This work demonstrates a deliberate attempt to significantly reduce the vaporization enthalpy of water through the introduction of weak water-amine hydrogen bond interactions in hydrogel evaporators. In this article, bio-based chitosan-agarose/multiwalled carbon nanotube hydrogel film evaporators (CAMFEs) exhibit larger vaporization enthalpy reduction with the presence of primary amine groups in chitosan. An interplay between vaporization enthalpy reduction and water diffusivity leads to an optimal ratio of chitosan to agarose = 7:1 (CAMFE7) showing an impressive evaporation rate of 4.13 kg $m^{-2}h^{-1}$ under 1 sun irradiation. CAMFE7 also exhibits excellent salt resistance, with a stable water evaporation rate, using brine water of up to 10% salinity under continuous 1 sun irradiation. The high mechanical robustness together with its scalability makes CAMFE7 a highly promising material for practical drinking water production.

**Keywords:** enthalpy reduction; solar evaporator; desalination; hydrogen bond; chitosan; amine

## 1. Introduction

Freshwater scarcity is becoming an increasingly pressing issue (Bremere, Kennedy, Stikker, & Schippers, 2001; Kalogirou, 2005; Tarazona-Romero, Campos-Celador, & Maldonado-Muñoz, 2022). The situation would only worsen with the global water demand projected to increase more than 55% by 2050 due to the rising population, along with the increasing industrial and agricultural activities (Shahzad, Burhan, Ang, & Ng, 2017). Comprising 97% of the earth's water, seawater is an inexhaustible water resource. Hence, many desalination technologies have been developed and some have advanced significantly, including the reverse osmosis (RO) technique which has become the mainstream desalination process. Nevertheless, the RO technique has its shortcomings, which typically require centralized facilities and huge infrastructure investment for plant and water grid development (Elimelech & Phillip, 2011; Gude & Fthenakis, 2020; Mathioulakis, Belessiotis, & Delyannis, 2007; Shahzad et al., 2017; Shannon et al., 2008; Z. Wang et al., 2019).

On the other hand, solar desalination offers a passive, off-grid, small-scale, and portable alternative (S. Guo et al., 2022; Tao et al., 2018; P. Wang, 2018; Zhang et al., 2019; Zhao, Guo, Zhou, Shi, & Yu, 2020). This brought about the development of photothermal devices, also known as solar evaporators, in recent years. These devices are meant to improve evaporation performance

through more efficient photothermal energy conversion and by reducing heat loss. However, the limited solar radiation and large vaporization enthalpy of water put a cap on the evaporation performance. This theoretical limit, previously coined as the "bulk water cap", was conservatively calculated to be ~1.7 kg $m^{-2}h^{-1}$, based on 100% photothermal conversion efficiency and the vaporization enthalpy of bulk water (Koh et al., 2021). Nevertheless, researchers have been seeking to overcome this limit through various methods, such as increasing the evaporation surface to tap into surrounding energy (Anukunwithaya et al., 2022; Gao, Wu, Wang, Owens, & Xu, 2021; Shao et al., 2020; Storer et al., 2020; Y. Wang et al., 2021; Xu et al., 2022) and reducing the enthalpy of water vaporization by disrupting the bulk water structure (Guo et al., 2020; Guo et al., 2019; Zhou, Guo, Zhao, & Yu, 2019; Zhou, Zhao, Guo, Rosenberger, & Yu, 2019).

It appears that reduction of water vaporization enthalpy is the only feasible path to break the theoretical limit of the "bulk water cap" without additional energy input. Several studies employing water-absorbing polymers including hydrogels and hydratable plastic solar evaporators to reduce water vaporization enthalpy have been reported (Y. Guo et al., 2022; Koh et al., 2021; Li et al., 2022; Lu et al., 2022; Lu et al., 2021; Yu et al., 2022). These polymers typically possess functional groups that are capable of disrupting the pristine bulk water hydrogen bonding structure leading to the reduction in vaporization enthalpy. In particular, it has been previously proposed that hydroxyl (−OH) groups in highly amorphous cellulose induce weaker cellulose-water hydrogen bonds (HBs) as compared to water-water HBs, resulting in a significant increase in evaporation performance (Koh et al., 2021). Therefore, it seems that there is a huge potential for further water vaporization enthalpy reduction through water-polymer interactions (Geng, Yang, & Wan, 2024). Nonetheless, the introduction of primary amine ($-NH_2$) groups in hydrogel-based solar evaporators possibly induces even weaker HB interaction at water-polymers interface.

Herein, $-NH_2$-induced weak HB for water vaporization enthalpy reduction was studied to improve the performance of solar evaporators. In particular, chitosan-agarose/multi-walled carbon nanotube hydrogel film evaporators (CAMFEs) with various chitosan and agarose content were fabricated as bio-based solar evaporators. The presence of $-NH_2$ groups in chitosan and −OH groups in both chitosan and agarose would allow the tailoring of HB strength between water and the polymers. Indeed, CAMFE with the ratio of chitosan to agarose = 7:1 (CAMFE7) achieves an impressive evaporation rate of 4.13 kg $m^{-2}h^{-1}$ under 1 sun irradiation. CAMFE7 also exhibits excellent salt resistance, having a stable evaporation rate of ~ 4 kg $m^{-2}h^{-1}$ when evaporating brine

water of up to 10% salinity for 6 h under continuous 1 sun irradiation. The practicality of employing CAMFE7 in a real situation is also demonstrated with homemade devices using large sheets of CAMFE7, showing the potential for upscaling the production of drinkable water. With its high rate of water production, salt resistance, and scalability, CAMFE7 is a promising photothermal evaporator for practical drinking water production.

## 2. Experimental section

### 2.1. Materials

Low molecular weight chitosan (Mw 50-190 kDa, 83% deacetylation), glacial acetic acid (ACS reagent, ≥99.7%), and sodium dodecyl sulfate (ACS reagent, ≥99.0%), sodium chloride (NaCl, ACS reagent, ≥99.9%), methylene blue (MB, ACS reagent, 82%), and methyl orange (MO, ACS reagent, 85%) were purchased from Sigma-Aldrich. Agarose (SeaKem®LE agarose, electrophoresis, gel strength >1,200 g/cm$^2$) was purchased from Lonza. Multi-walled carbon nanotube (−COOH 1.55% wt., >90.0%) was purchased from Cheaptubes. All chemicals were used without further purification. Milli-Q water (resistance ~18 MΩ) was used for all solution preparation throughout the experiment. Seawater was collected from West Coast Sea and filtered with Ø 0.45 μm filter paper prior to the tests.

### 2.2. Preparation of chitosan-agarose/multiwalled carbon nanotube hydrogel film evaporators (CAMFEs).

CAMFEs were fabricated with a modified method from previous work (Anukunwithaya et al., 2022). The fabrication process is briefly described as follows. To prepare a well-dispersed muti-walled carbon nanotubes (MWCNT) solution, 0.2% w/v of MWCNT and 0.1% w/v of sodium dodecyl sulfate (SDS) were dispersed in DI water using a homogenizer. Then 1.05% w/v of chitosan was added into the as-prepared MWCNT slurry. To dissolve chitosan completely, 1% v/v of acetic acid was added and stirred overnight. After that, 0.15% w/v of agarose was added to the black slurry to achieve a weight ratio of chitosan to agarose of 7:1. The black slurry was stirred at 80 ºC for 2 h before casting in a silicone mold (inner diameter of 0.045 m) with amount controlled to acquire thickness of 0.08 mm. The composite hydrogel film was cooled down for the gelation process and dried at 45ºC overnight. Finally, CAMFE7 was peeled and washed to remove acid and SDS residue. CAMFE1, 3, 5, and 9 were prepared with the same process at the proportional ratio of chitosan to agarose at 1:1, 3:1, 5:1, and 9:1, respectively. Also, chitosan/multiwalled carbon nanotube hydrogel film evaporator (CS-MW) was fabricated as

controlled samples without agarose whereas agarose/multiwalled carbon nanotube hydrogel film evaporators (Aga-MW) was prepared without the addition of chitosan and acetic acid. All the pure agarose, chitosan, and chitosan-agarose hydrogel film (AgaF, CSF, and CAFs, respectively) were prepared with the same condition with solar evaporator film samples for characterizations (See SI, Table S1).

### 2.3. Characterizations

Fourier-transform infrared spectroscopy (ATR-FTIR, Agilent; Cary 660 spectrometer with Pike Gladi ATR) was measured in the wavenumber range of 500 – 4000 $cm^{-1}$, with a resolution of 4 $cm^{-1}$ and 32 scans. The amine species of samples were collected using an x-ray photoelectron spectrometer (XPS, Kratos Analytical; Axis Supra.) with an A1 $K_\alpha$ x-ray source. The used spot size aperture in front of the electrostatic lenses and the analyzer pass energy of 25 eV, determined an instrumental resolution of 0.1 eV. The light absorption and reflection were carried out by an ultraviolet-visible-near infrared spectrometer (UV-vis-NIR, Agilent; Cary 5000). The temperature measurements and infrared images during solar evaporation test were taken by a digital thermometer (UNI-T; UT325D-K probe) and a thermal imaging camera (Seek, Shot Pro). Differential Scanning Calorimetry (DCS, TA instruments; DSC25) was conducted for pure water and fully-swollen samples for enthalpy of vaporization study with an opened pan. The crystallinity was observed by an x-ray diffractometer with Cu Kα radiation (XRD, Bruker; D8 advance). A polarized optical microscope (Nikon; Eclipse LV100ND) was used to obtain birefringent crystals. Surface morphological structure was characterized via scanning electron microscope (SEM, ZEISS; Supra40) with an accelerating voltage of 5.0 kV. The salinity of brine and purified water was determined by elemental analysis through an inductively coupled plasma-optical emission spectrometer (ICP-OES, Perkin Elmer Optima 5300DV), and Decolorization of MB and MO of wastewaters and purified water were measured by an ultraviolet-visible spectrometer (UV-vis, Shimadzu; UV-1800).

### 2.4. Solar evaporation test setup.

DI water, simulated seawater (3.5, 10, and 25% wt. NaCl solution), actual seawater, and organic dye wastewaters were used for the solar evaporation tests. The evaporation experiment in the lab test was conducted using a solar simulator (Honle; Sol500 with AM1.5G filter). The illumination intensity was calibrated to 1 kW $m^{-2}$ or 1 sun, using a thermopile (Newport; PVM914), connected to a power meter (Newport; 91150). The mass change of water was automatically

recorded by an electronic balance (Sartorius; EnrisII with a resolution of 0.001 g) every 10 min. All the evaporation experiments were performed at ~27 ± 2 ºC and relative humidity of ~50 ± 5 %.

For the outdoor test, the water collection was carried out under an ambient environment, an open area at College of Design and Engineering, National University of Singapore (NUS), Singapore (at the latitude of 1.2980439° / longitude of 103.7718327°). The solar irradiance and temperature were measured with a thermopile (Newport; PVM914), connected to a power meter (Newport; 91150). The outdoor experiment was conducted from 8:00 to 17:00.

## 3. Results and discussion

### 3.1. Fabrication of chitosan-agarose/multi-walled carbon nanotube hydrogel film evaporators (CAMFEs)

CAMFEs and other sample films were fabricated through a facile method as illustrated in Fig. 1 and Table S1 with chitosan, agarose, and MWCNT as the main components. The chemical compositions of the composite films were analyzed by fourier transform infrared (FT-IR) spectroscopy. For AgaF, broad band of O-H stretching is presented in the range of 3100 – 3700 $cm^{-1}$, and that of O-H bending is shown at 1645 $cm^{-1}$. In addition, the characteristic peaks at 880, 930, and 990 are presented according to 3,6-anhydrogalactose linkage (Ang, Tan, & Chew, 2019; Chaudhary, Nataraj, Gogda, & Meena, 2014; Chaudhary, Vadodariya, Nataraj, & Meena, 2015). Each agarose molecule forms double helices in solution, where adjacent chains are held together by HBs between the −OH groups on the sugar units. These helices further aggregate to form a gel network through additional hydrogen bonding interactions. For CSF, the board bands at 3000 – 3700 $cm^{-1}$ are attributed to N-H and O-H stretching vibration. Also, the peaks at 1540, and 1650 $cm^{-1}$ are represented by secondary amide and C=O stretching, respectively (Chaudhary et al., 2014; Chaudhary et al., 2015). Likewise, the chemical compositions of CAF1, 3, 5, 7, and 9, presenting the main functional group of both chitosan and agarose as shown in Fig.1b. According to Fig. 1c, CS powder shows characteristic peaks at 1570 $cm^{-1}$ representing primary amine, and those peaks for CAMFEs were shifted to lower wavenumber around 1548 – 1554 $cm^{-1}$, due to the formation of intermolecular HB between the $–NH_2$ group of chitosan and –OH group of agaroses. It has also been reported that the chitosan-agarose interactions significantly interferes with the formation of ordered agarose conformations and structures (Trivedi, Rao, & Kumar, 2014). Additionally, $–NH_2$ would be protonated by acetic acid into $–NH_3^+$, showing overlapped peaks (Huang et al., 2018).

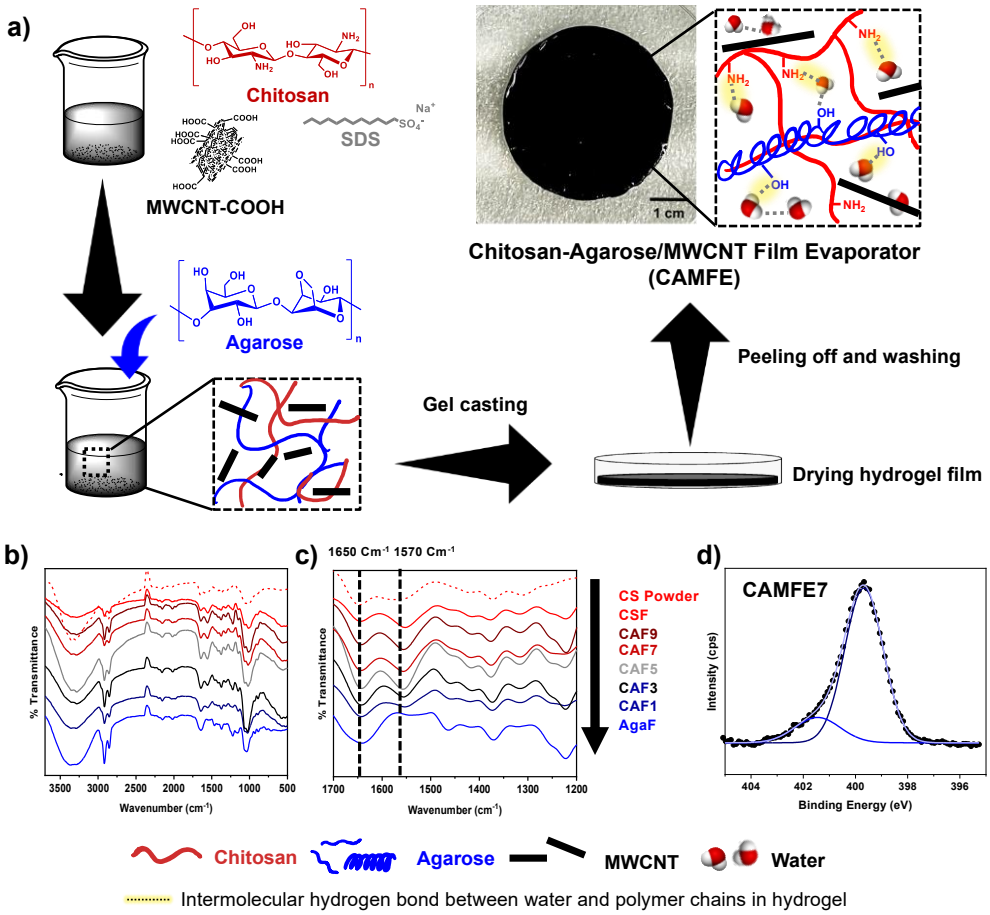


**Fig. 1.** Fabrication and structure of CAMFEs. a) Schematic diagram of CAMFEs preparation and proposed structure of CAMFEs in the swollen state with intermolecular HB between water and polymer chains in hydrogel; FT-IR spectra in the range between b) 500 – 3700 $cm^{-1}$ and c) 1200 – 1700 $cm^{-1}$ where CS powder is indicated to raw chitosan powder; d) XPS spectrum of CAMFE7.

As such, it is possible that free protonated $–NH_3^+$ could bind to $–COO^-$ through electrostatic interaction and crosslink to keep the charge-balanced, indicated by the C=O stretching of amide group at 1650 $cm^{-1}$ was lowering to 1644 $cm^{-1}$ for CAFs (Ghosh & Ali, 2012). Importantly, both chitosan and agarose homogenously blend and form HB with each other (Fig. S1c). The interpenetrating network of polymer composites could be indicated as the clear films shown in Fig. S1d. In addition, the dominance of $–NH_2$ groups over $–NH_3^+$ at the surface of CAMFE7 was also confirmed through X-ray photoelectron spectroscopy (XPS) (Fig. 1d).

### 3.2. Water evaporation performances of CAMFEs

The water evaporation performance of CAMFEs along with other controls was measured using the setup (Fig. S2a) that includes a polyethylene foam as a floating insulator, an aluminum cover to reflect irradiation outside of the material, and water-wicked cellulose papers to transport

water from the reservoir to the evaporator (Fig. S2b). The thickness of all samples was controlled at 0.080 ± 0.01 mm. Under 1 sun irradiation, the water evaporation rates and mass changes of the samples are presented in Fig. 2a-b. Aga-MW, CAMFE1, 3, 5, 7, 9, and CS-MW exhibited impressive performances with steady-state evaporation rates of 2.69, 3.17, 3.33, 3.64, 4.13, 3.06, and 3.33 kg $m^{-2}h^{-1}$, respectively (Fig. 2c). Such a high evaporation rate can be partially attributed to the effective solar absorption from the incorporation of MWCNT as the solar absorber. As a

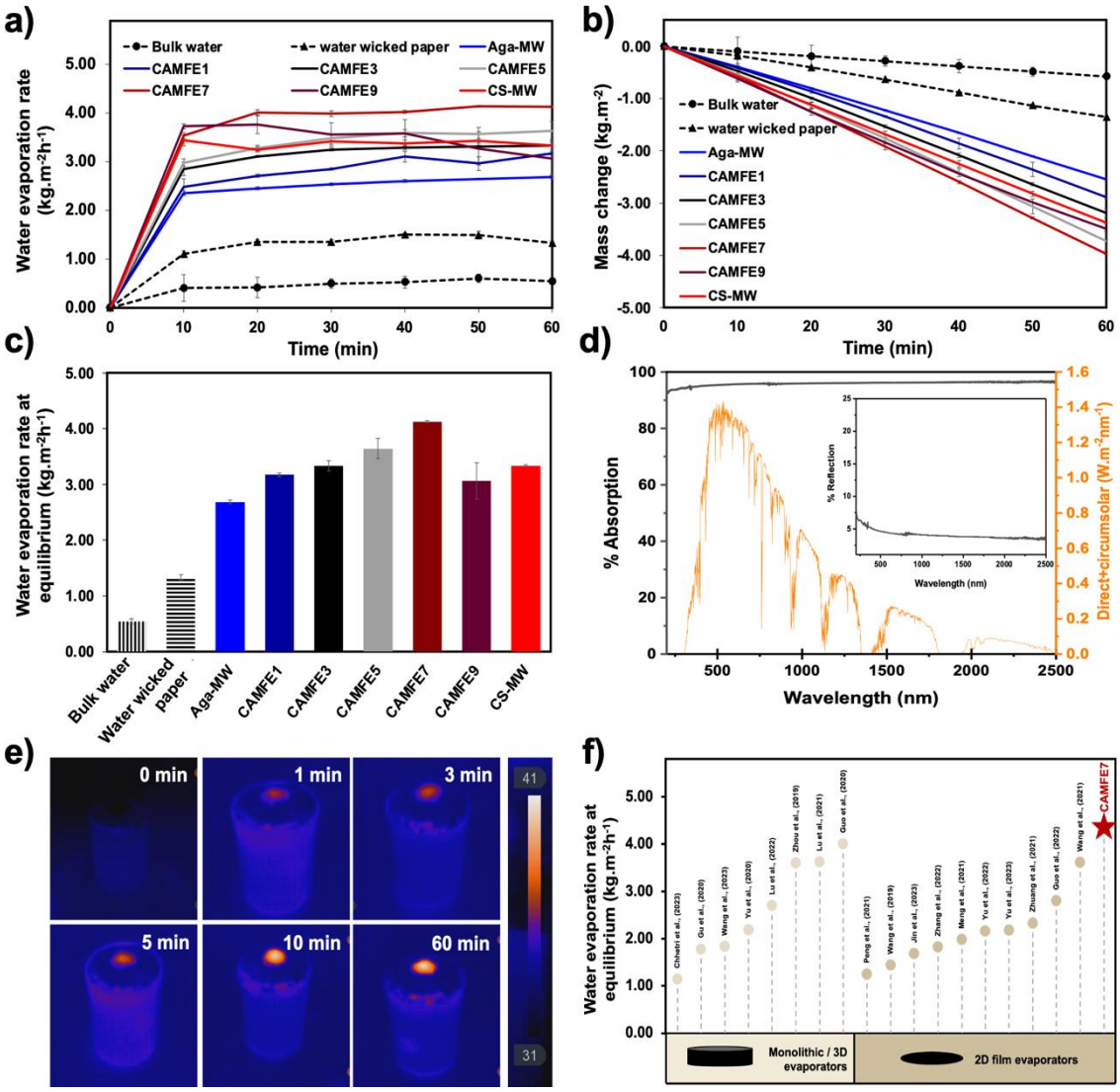


**Fig. 2. Solar evaporation performance of CAMFEs under 1 sun irradiation.** a) Water evaporation rate and b) mass change during 1-h evaporation test of CAMFEs and controls; c) The evaporation rate at equilibrium of CAMFEs and controls; d) %absorption and reflectance of swollen CAMFE7 with simulated solar spectrum under AM 1.5G; e) Thermal infrared images of CAMFE7 during 1-h evaporation test; f) The comparison performance between our CAMFE7 and other works.

result, CAMFEs and their controls exhibit more than 96% absorption in the entire range of wavelength from 200 to 2500 nm (Fig. 2d and Fig. S2c-h). Such an excellent solar absorption of CAMFE7, it leads to surface temperature rising between 37 and 39.9 °C upon 1 sun irradiation (Fig. 2e). Indeed, with an evaporation rate of 4.13 kg $m^{-2}$ $h^{-1}$, CAMFE7's performance is remarkable compared to other 2D film evaporators found in literature, and even some 3D structured evaporators that tap on surrounding energy (Fig. 2f).

### 3.3. Reduction of vaporization enthalpy by amine-induced weak hydrogen bonding

However, excellent photothermal conversion alone cannot explain the remarkable performance of the evaporators, since the evaporation rate exceeds that of the bulk water cap of 1.7 kg $m^{-2}$ $h^{-1}$ (See SI, Eq. S3.) (Koh et al., 2021). Indeed, all the samples exhibit water vaporization enthalpy reduction ability due to the disruption of the bulk water structure through carbohydrate polymer-water interactions. Differential scanning calorimetry (DSC) measurement (Fig. 3a) showed that water vaporization enthalpy of bulk water, Aga-MW, CAMFE1, 3, 5, 7, 9 and CS-MW are 2243, 1950, 1911, 1866, 1740, 1676, 1434, and 1258 J/g, respectively (Fig. 3b). The obtained values of equivalent evaporation enthalpy of water in CAMFEs, Aga-MW, and CS-MW by experimental measurement also shows a similar trend to DSC results (Fig. S3c). With that, their respective photothermal conversion efficiency under 1-sun irradiation is presented in Fig. S4. These results suggest that increasing chitosan content in CAMFEs would typically lead to a decrease in water vaporization enthalpy, thereby reducing the amount of energy required to evaporate per unit of water. Despite the increase in chitosan content, the evaporation rate reached a peak at 4.13 kg $m^{-2}h^{-1}$ for CAMFE7. With CAMFE9 and CS-MW, the evaporation rates are slightly lower at 3.06 and 3.33 kg $m^{-2}h^{-1}$ under 1 sun irradiation. This is due to the poor water transport mechanism which will be discussed in a subsequent section.

The reduction in water vaporization enthalpy with increased chitosan content can be attributed to the different chemical groups possessed by 2 polysaccharides, namely the $–NH_2$ and –OH groups. More importantly, the primary difference between the $–NH_2$ and –OH groups lie in their heteroatom. N (3) is less electronegative than O (3.5) leading to a less polar N-H bond where N and H have a smaller negative and positive charge, respectively. Indeed, the strength of HB can be somewhat predicted from the attractive force between a hydrogen atom covalently bonded to a very electronegative atom in the order of F > O > N > C (Chaplin, 2007; Pauling, 1932; Simončič

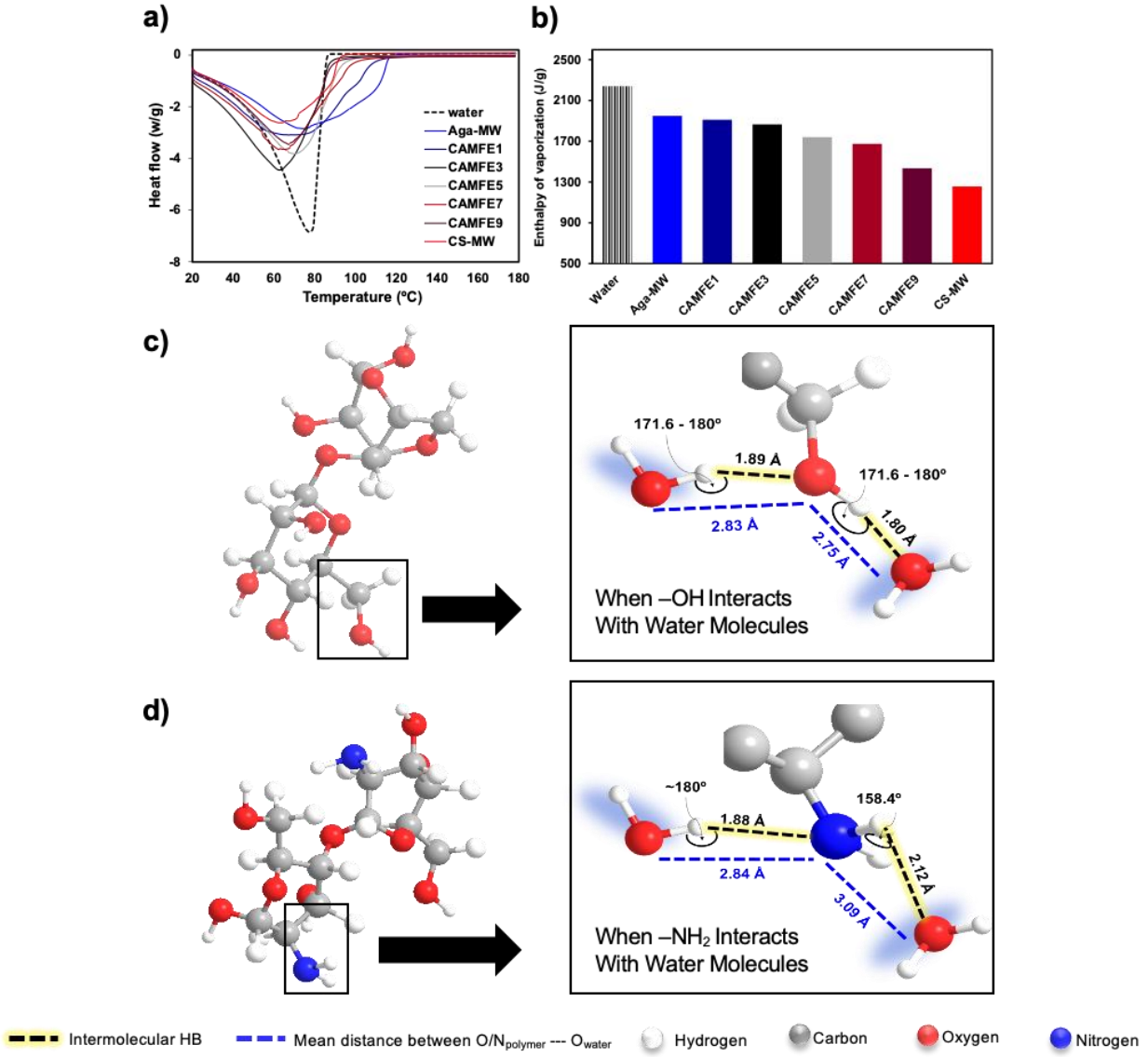


**Fig. 3. Lowering enthalpy related weaker intermolecular HB interaction.** a) Thermogram of bulk water, CAMFEs, and controls with heat flow mW/°C; b) The measured vaporization enthalpy by DSC; c) A repeating unit of D-galactose and 3,6-anhydro L-galactose and intermolecular HB length and angle between –OH and water molecules; d) A repeating unit of glucosamine and intermolecular HB length and angle between –$NH_2$ and water molecules.

& Urbic, 2018). Moreover, the effect of –$NH_2$-induced weaker HB can be easily observed from the lower boiling of primary amines as compared to their alcohol analogs (e.g. methylamine and methanol) (Hladílková, Fischer, Jungwirth, & Mason, 2015). Both functional groups possess 3 HB sites, –$NH_2$ has 1 N-acceptor (1 lone pair) and 2 H-donor sites, whereas –OH has 2 O-acceptors (2 lone pairs) and 1 H-donor site. However, previous simulation studies have revealed that –$NH_2$ is a better HB acceptor than a donor, whereas the opposite is true for –OH (Rablen, Lockman, &

Jorgensen, 1998). These studies have also shown that $–NH_2$ as the HB acceptor can form stronger HB with water, as compared to –OH being the HB donor to water. However, the $–NH_2$ weak HB donor ability also led to difficulties in locating the minimum energy conformation (Jorgensen & Gao, 1986; Rizzo & Jorgensen, 1999). As illustrated in Fig. 3c and 3d, this is supported by a longer HB length and a larger deviation from linearity in HB angle as presented in Table S2. In fact, it has been concluded that $–NH_2$ as a weaker HB donor more than compensates for it being a stronger HB acceptor (Nagy, III, & Nicholas, 1989; Rizzo & Jorgensen, 1999).

### 3.4. Water diffusion within the interpenetrated polymer network

The photothermal conversion and water vaporization enthalpy are not the only factors governing the evaporation performance of solar evaporators. This can be observed from the poorer performance of CAMFE9 and CS-MW as compared to CAMFE7, with an evaporation rate of only slightly over 3 $m^{-2}h^{-1}$, despite having more $–NH_2$ groups (The water evaporation rate of CAMFE9 is referred to Fig. S5). Sufficient water transport from the water reservoir to the top evaporating surface has always been a crucial factor affecting solar desalination systems. Since CAMFEs do

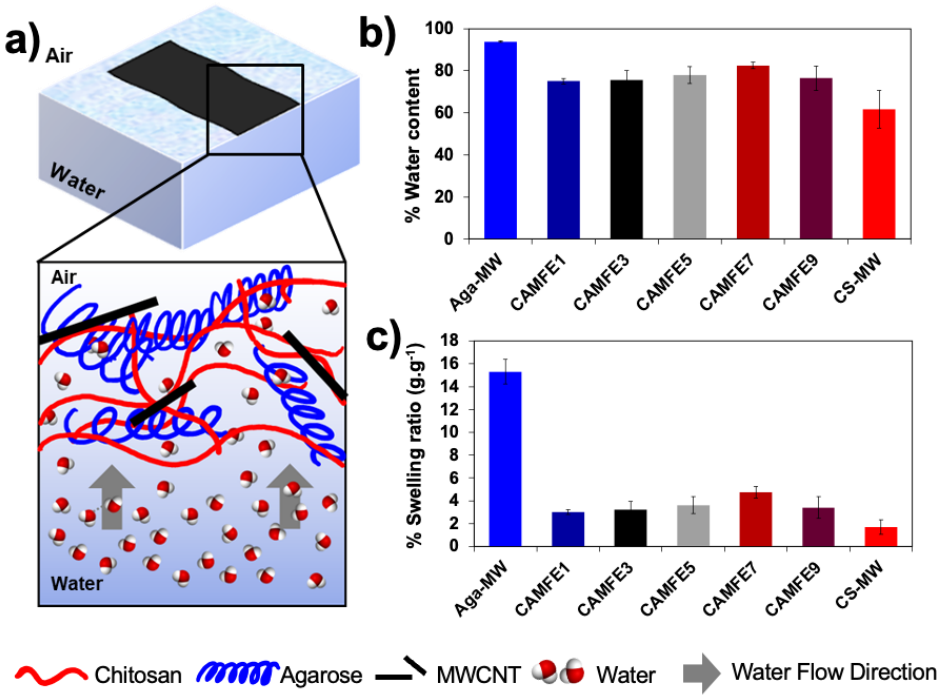


**Fig. 4. Water transport related diffusivity, and water absorptivity of CAMFEs, Aga-MW, and CS-MW.** a) Schematic diagram for water diffusion and transport from the bottom to the top of the evaporator; b) Water content of CAMFEs, Aga-MW, and CS-MW; c) The swelling ratio of CAMFEs, Aga-MW, and CS-MW.

not have a sponge-like porous morphology as shown in the SEM images (Fig. S6), along with the absence of chitosan crystals (Fig. S7), water is transported through diffusion within the interpenetrated polymer network as illustrated in Fig. 4a. Even though the water transport through the hydrogel films would be much slower than water pump through porous materials, CAMFE7 show remarkable water evaporation rate with an optimal ratio of $–NH_2$ and –OH groups. Additionally, the water contents and swelling ratio of the samples at their saturated state are presented in Fig. 4b-c. Aga-MW shows the highest water content, at 94%wt., whereas CS-MW only shows 68%wt. This indicates that chitosan alone could not absorb water as much as Aga-MW or their blends (i.e. CAMFEs). Once chitosan was incorporated with agarose in CAMFEs, the absorbed water in CAMFEs moderately decreased to 76-82 %wt. for CAMFE1, 3, 5, and 7. A slight increase in absorbed water from 76% in CAMFE1 to 82% in CAMFE7 can also be observed. This could possibly be due to a larger disruption to the ordered helical chain conformations of Aga chains at lower Aga content given its interaction with chitosan chains (Fig. 1c) (Trivedi et al., 2014). A less ordered structure could lead to more interaction sites with water, which are beneficial for water absorption(Gómez-Mascaraque, Méndez, Fernández-Gutiérrez, Vázquez, & San Román, 2014; Vardar, Vert, Coudane, Hasirci, & Hasirci, 2012). In general, with a lower absorbed water content, water channels within the hydrogels would shrink, and water molecules would have to travel a more tortuous path to reach the evaporating surface (Koh et al., 2019). Previous studies have shown that lower absorbed water content in hydratable polymers has a positive relationship with tortuosity of water travel paths and a negative effect on water's diffusivity, thereby leading to poorer transport within the polymer network (Kulasinski, Guyer, Derome, & Carmeliet, 2015; Kulasinski & Guyer, 2016; Kulasinski et al., 2014). Therefore, an appropriate ratio of chitosan and agarose is necessary to achieve an optimal balance between water vaporization enthalpy reduction, water diffusivity, and hydrophilicity, so as to achieve high evaporation rates.

### 3.5. Solar desalination and stability of CAMFE7

Apart from evaporation performance, salt resistance is another key property of solar evaporators. Salt resistance would allow the evaporators to run autonomously, reducing the need for human interventions to remove accumulated salt (e.g. washing) (Anukunwithaya et al., 2022; Chen et al., 2021; Kuang et al., 2019; Zhang, Xiong, Nandakumar, & Tan, 2020; Y. Zhang et al., 2020). As such, solar desalination tests were conducted using saline water of 3.5, 10, and 25% salinity; moreover, CAMFE7 shows a stable water evaporation rate in the range of ~ 4 kg $m^{-2}h^{-1}$

under 3.5 and 10% salinity continuously for 6 h under 1 sun irradiation without salt precipitation on its surface (Fig. 5a and 5b). However, salt precipitation occurred during the desalination process with 25% salinity (Fig. 5c), which leads to a gradual decrease in water evaporation rate, due to the reduction in photothermal effect as the white crystals interfere with the interaction between light and solar absorbers, along with a reduction in effective evaporation area. Nevertheless, CAMFE7 performs well with actual seawater with ~ 3.5% salinity. Solar desalination of seawater water was

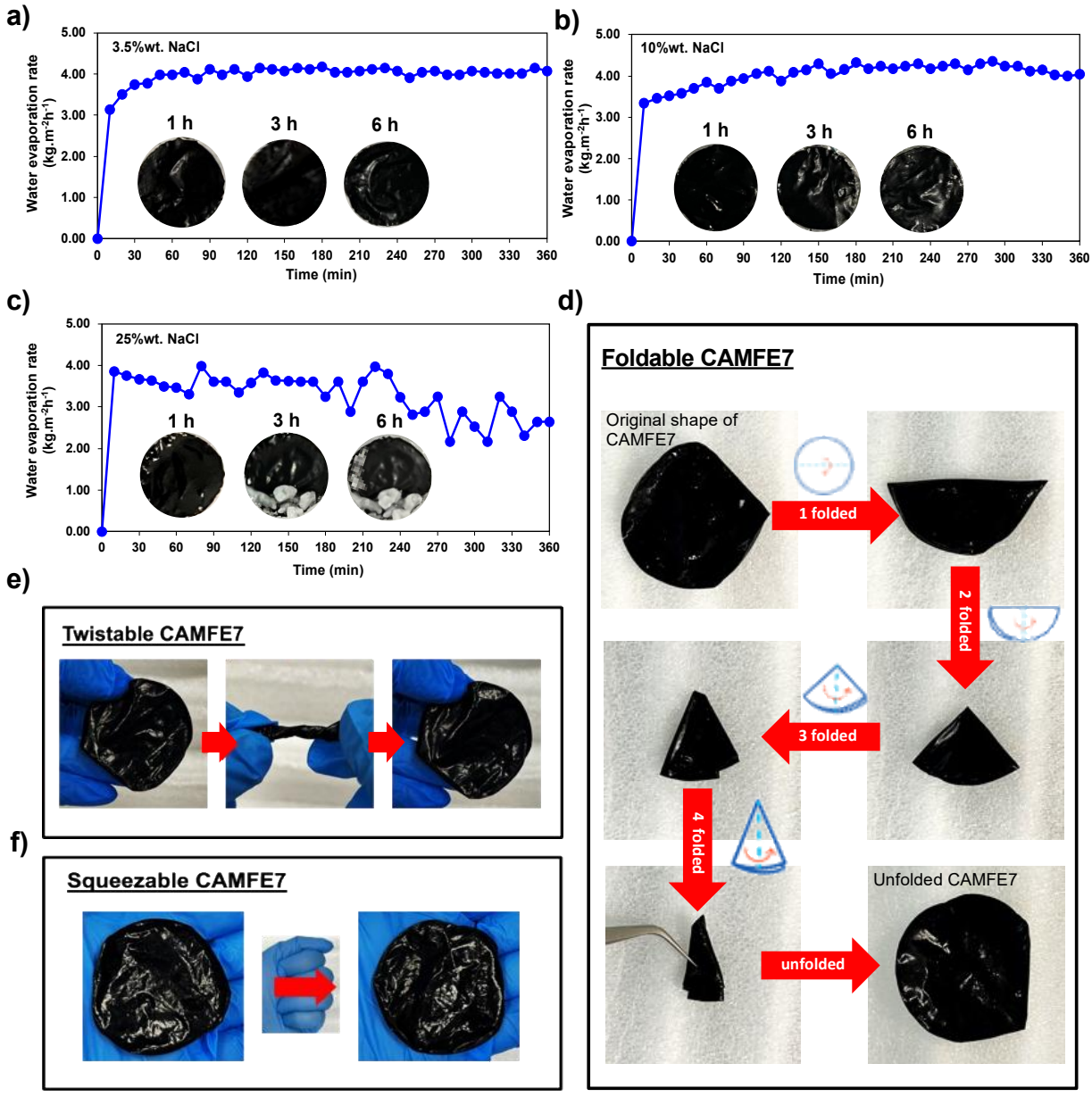


**Fig. 5 Solar desalination test of CAMFE7 with saline water.** The solar desalination test and observation of salt precipitation toward; a) 3.5%, b) 10%, and c) 25% salinity; Mechanical robustness of CAMFE7 by d) folding, e) twisting, and f) squeezing.

carried out for 8 h under 1 sun irradiation for 7 consecutive days to confirm its long-term stability. It exhibits evaporation rate in the range of 3 - 4 kg $m^{-2}h^{-1}$ with self-regeneration ability within 16 h of downtime in the ambient environment (Fig. S8). The mechanism for self-regeneration can be attributed to the interconnected water pathways that allow for ion exchange to take place (Anukunwithaya et al., 2022; Cao et al., 2021; Koh et al., 2021; Liu et al., 2021).

Besides, the practicality of applying CAMFE7 in actual applications also lies in its mechanical robustness, which allow for easy handling, storage, and transportation. After folding (Fig.5d), twisting (Fig.5e), and squeezing (Fig.5f), CAMFE7 remained intact and presented the same appearance as the initial state of swollen CAMFE7. On the other hand, some hydrogels, such as Aga-MW are too brittle for practical application, which disintegrate easily upon experiencing slight mechanical forces and deformation (Fig S9).

### 3.6. Practical usage of CAMFE7 and wastewater treatment

As aforementioned, CAMFE7 shows the possibility of upscaling CAMFE7 fabrication with easily produced large sheets (Fig. 6a). This would allow CAMFE7 to be conveniently employed in larger solar stills of various designs, such as the one illustrated in Fig. 6b, thereby upscaling water production to a practical level. To demonstrate its practicality in real situations, a homemade device utilizing CAMFE7 with a diameter of 10 cm was fabricated and set for an outdoor desalination test between 08.00 to 17.00 on a partially cloudy day (Fig. S10a-d). The various environmental factors including solar intensity, temperature, and humidity are presented in Fig. S10e. Deviations in evaporation performance from simulated 1 sun laboratory are expected and can be largely attributed to various factors, affecting the solar irradiation intensity, such as solar incidence angle at different times of the day and the movement of passing clouds. Nevertheless, the result shows that with further upscaling, a square meter of CAMFE7 would be able to produce ~4 L of drinkable water even on such a partially cloudy day, which would be in fact sufficient for 2 adults in a day.

Indeed, the water collected from the solar still indicates that the concentration of various ions decreased by 3 to 4 magnitudes, meeting the drinking water standard of the World Health Organization (WHO) (Fig. 6c). Other than saline water, water containing 20 ppm of MO (anionic dye) and 10 ppm of MB (cationic dye) were prepared as models for industrial wastewater purification tests. Indeed, CAMFE7 has the ability to separate and purify water contaminated with

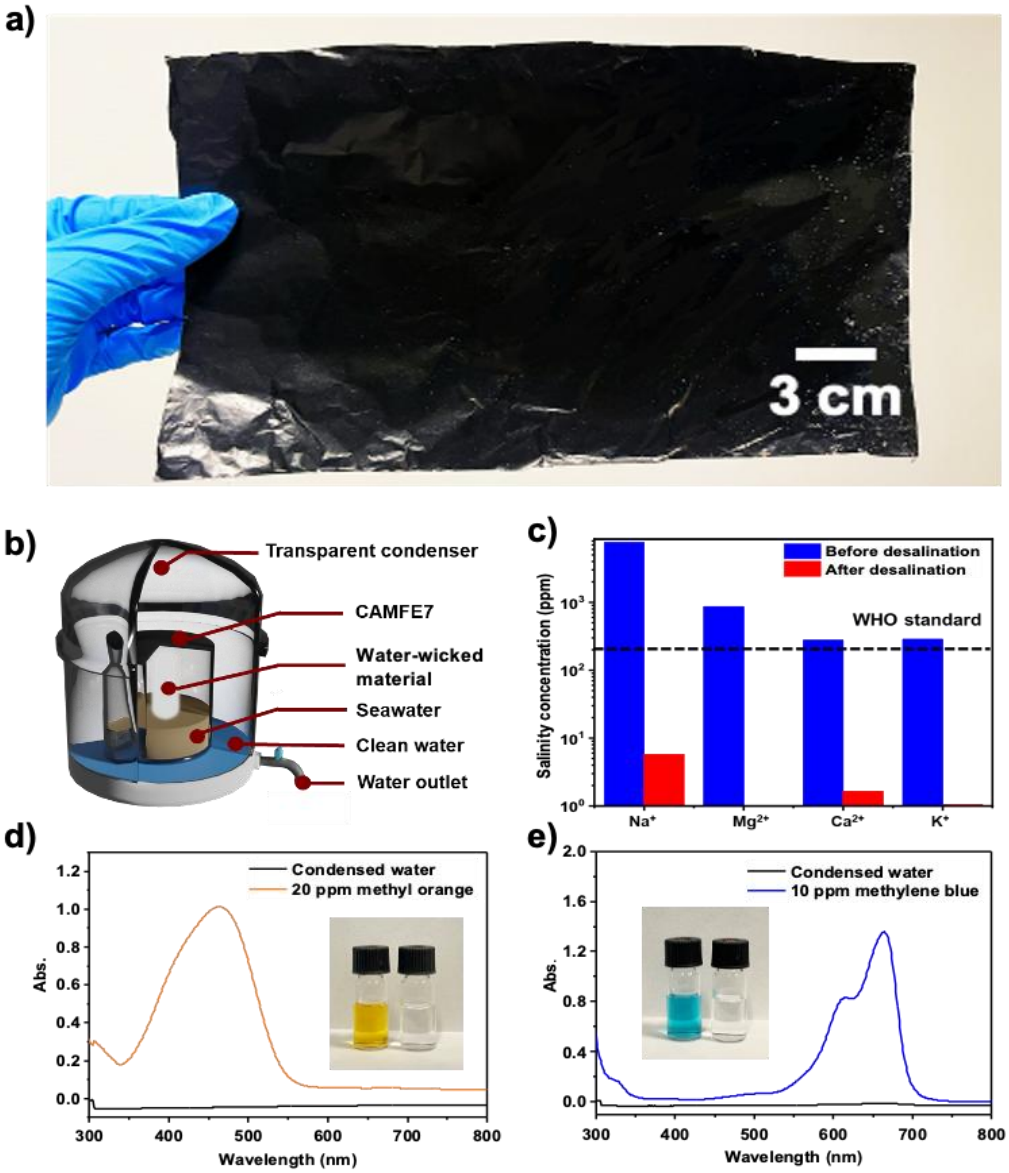


**Fig. 6. Scalability for practical usage of CAMFE7 toward seawater and wastewater.** a) The scalable CAMFE7; b) Schematic demonstration of desalination tank; c) The solar desalination with muti ions in actual seawater; The wastewater treatment used d) 20 ppm of methyl orange and e) 10 ppm of methylene blue.

organic molecules, indicating that their applicability could go beyond desalination, and be employed in wastewater treatment applications. (Fig. 6d-e).

## 4. Conclusion

In summary, the vaporization enthalpy of water in hydrogel evaporators can be lowered significantly with the incorporation of chitosan due to its $–NH_2$ functional groups, which induces weak hydrogen bonding with water. However, chitosan's poorer affinity with water led to poorer

water absorption, and hence, lower water diffusivity. On the other hand, the more hydrophilic agarose can provide better water transport to the evaporating surface. To achieve an optimal balance between enthalpy reduction and water diffusivity, the proportion of $–NH_2$ and –OH functional groups within the interpenetrated network of the chitosan-agarose hydrogel can be manipulated, by tuning their composition. Indeed, an optimal 7:1 ratio of chitosan to agarose (CAMFE7) exhibited a remarkable water evaporation rate of 4.13 kg $m^{-2}h^{-1}$, which is an extremely high performance among 2D evaporators. CAMFE7 also exhibits excellent salt resistance with a stable water evaporation rate of about ~ 4 kg $m^{-2}h^{-1}$, up to 10% salinity within 6 h under 1 sun irradiation. The continuous solar desalination test employing CAMFE7 also shows an evaporation rate of 3 – 4 kg $m^{-2}h^{-1}$ with self-regeneration abilities. Moreover, CAMFE7 boasts scalability and mechanical robustness, positioning it as a highly promising material for practical water treatment applications. A homemade device was fabricated to demonstrate CAMFE7's ability to collect clean water using natural solar irradiation on a partially cloudy day, indicating its strong potential for further upscaling of drinking water production.

## CRediT authorship contribution statement

**Patsaya Anukunwithaya**: Conceptualization, Methodology, Validation, Investigation, Formal analysis, Writing – original draft, Writing – review & editing. **Nanxue Liu**: Validation, Investigation, Formal analysis. **Siqi Liu**: Investigation, Formal analysis. **Eknarin Thanayupong**: Investigation, Formal analysis. **Lili Zhou**: Investigation, Formal analysis. **Nuttaporn Pimpha**: Investigation, Formal analysis. **Jiakang Min**: Investigation, Formal analysis. **Wannee Chinsirikul:** Writing—review & editing. **Warintorn Thitsartarn:** Funding acquisition **Junqiang Justin Koh:** Conceptualization, Writing – review & editing, Supervision. **Chaobin He** Conceptualization, Writing – review & editing, Supervision, Funding acquisition.

## Declaration of Competing Interest

The authors declare that they have no known competing financial interests or personal relationships that could have appeared to influence the work reported in this paper.

## Data availability

Data will be made available on request.


## Acknowledgment

We thank the National Nanotechnology Center (NANOTEC-NSTDA) and Royal Thai Government Scholarship (OCSC), Thailand, for fully funding the Ph.D. scholarship to Patsaya

Anukunwithaya. This project was partially supported by RIE2025 MTC Young Individual Research Grant (Grant no. M22K3c0101), administered by Agency of Science, Technology and Research (A*STAR), and a grant from A*STAR IMRE – SCG Chemicals Advanced Composite Joint Lab (grant number I1801E0024). We are also thankful to Mr. Pinyawee Songkhum for informative graphic work.

**Appendix A. Supporting information**

Supplementary data associated with this article can be found in the online version at https://doi.org...

**References**

Ang, E. H., Tan, Y. Z., & Chew, J. W. (2019). A three-dimensional plasmonic spacer enables highly efficient solar-enhanced membrane distillation of seawater. *Journal of Materials Chemistry A,* 7(17), 10206-10211.

Anukunwithaya, P., Koh, J. J., Chuan Yeo, J. C., Liu, S., Hou, X., Liu, N., & He, C. (2022). A self-regenerating 3D sponge evaporator with a tunable porous structure for efficient solar desalination. *Journal of Materials Chemistry A,* 10(29), 15743-15751.

Bremere, I., Kennedy, M., Stikker, A., & Schippers, J. (2001). How water scarcity will effect the growth in the desalination market in the coming 25 years. *Desalination,* 138(1), 7-15.

Cao, S., Wu, X., Zhu, Y., Gupta, P., Martinez, A., Zhang, Y., . . . Singamaneni, S. (2021). MXene aerogel for efficient photothermally driven membrane distillation with dual-mode antimicrobial capability. *Journal of Materials Chemistry A,* 9(39), 22585-22596.

Chaplin, M. (2007). Water's Hydrogen Bond Strength. *ArXiv,* 706.

Chaudhary, J. P., Nataraj, S. K., Gogda, A., & Meena, R. (2014). Bio-based superhydrophilic foam membranes for sustainable oil–water separation. *Green Chemistry,* 16(10), 4552-4558.

Chaudhary, J. P., Vadodariya, N., Nataraj, S. K., & Meena, R. (2015). Chitosan-Based Aerogel Membrane for Robust Oil-in-Water Emulsion Separation. *ACS Applied Materials & Interfaces,* 7(44), 24957-24962.

Chen, X., He, S., Falinski, M. M., Wang, Y., Li, T., Zheng, S., . . . Ren, Z. J. (2021). Sustainable off-grid desalination of hypersaline waters using Janus wood evaporators. *Energy & Environmental Science,* 14(10), 5347-5357.

Chhetri, S., Nguyen, A. T., Song, S., Gaillard, N., Severa, G., Ma, T., . . . Lee, W. (2023). Flexible Graphite Nanoflake/Polydimethylsiloxane Nanocomposites with Promising Solar–Thermal Conversion Performance. *ACS Applied Energy Materials,* 6(4), 2582-2593.

Elimelech, M., & Phillip, W. A. (2011). The Future of Seawater Desalination: Energy, Technology, and the Environment. *Science,* 333(6043), 712-717.

Gao, T., Wu, X., Wang, Y., Owens, G., & Xu, H. (2021). A Hollow and Compressible 3D Photothermal Evaporator for Highly Efficient Solar Steam Generation without Energy Loss. *Solar RRL,* 5(5), 2100053.

Geng, X., Yang, P., & Wan, Y. (2024). How to reduce enthalpy in the interfacial solar water generation system for enhancing efficiency? *Nano Energy,* 123, 109434.

Ghosh, A., & Ali, M. A. (2012). Studies on physicochemical characteristics of chitosan derivatives with dicarboxylic acids. *Journal of Materials Science,* 47(3), 1196-1204.

Gómez-Mascaraque, L. G., Méndez, J. A., Fernández-Gutiérrez, M., Vázquez, B., & San Román, J. (2014). Oxidized dextrins as alternative crosslinking agents for polysaccharides: Application to hydrogels of agarose–chitosan. *Acta Biomaterialia,* 10(2), 798-811.

Gu, Y., Mu, X., Wang, P., Wang, X., Liu, J., Shi, J., . . . Miao, L. (2020). Integrated photothermal aerogels with ultrahigh-performance solar steam generation. *Nano Energy,* 74, 104857

Gude, V. G., & Fthenakis, V. (2020). Energy efficiency and renewable energy utilization in desalination systems. *Progress in Energy,* 2(2), 022003.

Guo, S., Zhang, Y., Qu, H., Li, M., Zhang, S., Yang, J., . . . Tan, S. C. (2022). Repurposing face mask waste to construct floating photothermal evaporator for autonomous solar ocean farming. *EcoMat,* 4(2), e12179.

Guo, Y., de Vasconcelos, L. S., Manohar, N., Geng, J., Johnston, K. P., & Yu, G. (2022). Highly Elastic Interconnected Porous Hydrogels through Self-Assembled Templating for Solar Water Purification. *Angewandte Chemie International Edition,* 61(3), e202114074.

Guo, Y., Zhao, X., Zhao, F., Jiao, Z., Zhou, X., & Yu, G. (2020). Tailoring surface wetting states for ultrafast solar-driven water evaporation. *Energy & Environmental Science,* 13(7), 2087-2095.

Guo, Y., Zhou, X., Zhao, F., Bae, J., Rosenberger, B., & Yu, G. (2019). Synergistic Energy Nanoconfinement and Water Activation in Hydrogels for Efficient Solar Water Desalination. *ACS Nano,* 13(7), 7913-7919.

Hladílková, J., Fischer, H. E., Jungwirth, P., & Mason, P. E. (2015). Hydration of Hydroxyl and Amino Groups Examined by Molecular Dynamics and Neutron Scattering. *The Journal of Physical Chemistry B,* 119(21), 6357-6365.

Huang, H., Liu, M., Jiang, R., Chen, J., Huang, Q., Wen, Y., . . . Wei, Y. (2018). Fabrication and characterization of hyperbranched polyglycerol modified carbon nanotubes through the host-guest interactions. *Materials Science and Engineering C,* 91, 458-465.

Jin, M., Qu, X., Li, J., Deng, L., Han, Z., Chen, S., & Wang, H. (2023). Bacterial cellulose-based film with self-floating hierarchical porous structure for efficient solar-driven interfacial evaporation. *Carbohydrate Polymers,* 321, 121324.

Jorgensen, W. L., & Gao, J. (1986). Monte Carlo simulations of the hydration of ammonium and carboxylate ions. *The Journal of Physical Chemistry,* 90(10), 2174-2182.

Kalogirou, S. A. (2005). Seawater desalination using renewable energy sources. *Progress in Energy and Combustion Science,* 31(3), 242-281.

Koh, J. J., Lim, G. J. H., Chakraborty, S., Zhang, Y., Liu, S., Zhang, X., . . . He, C. (2021). Robust, 3D-printed hydratable plastics for effective solar desalination. *Nano Energy,* 79, 105436.

Koh, J. J., Lim, G. J. H., Zhou, X., Zhang, X., Ding, J., & He, C. (2019). 3D-Printed Anti-Fouling Cellulose Mesh for Highly Efficient Oil/Water Separation Applications. *ACS Applied Materials & Interfaces,* 11(14), 13787-13795.

Kuang, Y., Chen, C., He, S., Hitz, E. M., Wang, Y., Gan, W., . . . Hu, L. (2019). A High-Performance Self-Regenerating Solar Evaporator for Continuous Water Desalination. *Advanced Materials,* 31(23), 1900498.

Kulasinski, K., Guyer, R., Derome, D., & Carmeliet, J. (2015). Water Diffusion in Amorphous Hydrophilic Systems: A Stop and Go Process. *Langmuir,* 31(39), 10843-10849.

Kulasinski, K., & Guyer, R. A. (2016). Quantification of Nanopore Networks: Application to Amorphous Polymers. *The Journal of Physical Chemistry C,* 120(49), 28144-28151.

Kulasinski, K., Keten, S., Churakov, S. V., Guyer, R., Carmeliet, J., & Derome, D. (2014). Molecular Mechanism of Moisture-Induced Transition in Amorphous Cellulose. *ACS Macro Letters,* 3(10), 1037-1040.

Li, X.-P., Li, X., Li, H., Zhao, Y., Wu, J., Yan, S., & Yu, Z.-Z. (2022). Reshapable MXene/Graphene Oxide/Polyaniline Plastic Hybrids with Patternable Surfaces for Highly Efficient Solar-Driven Water Purification. *Advanced Functional Materials,* 32(15), 2110636.

Liu, K., Zhang, W., Cheng, H., Luo, L., Wang, B., Mao, Z., . . . Feng, X. (2021). A Nature-Inspired Monolithic Integrated Cellulose Aerogel-Based Evaporator for Efficient Solar Desalination. *ACS Applied Materials & Interfaces,* 13(8), 10612-10622.

Loo, S.-L., Vásquez, L., Paul, U. C., Campagnolo, L., Athanassiou, A., & Fragouli, D. (2020). Solar-Driven Freshwater Generation from Seawater and Atmospheric Moisture Enabled by a Hydrophilic Photothermal Foam. *ACS Applied Materials & Interfaces,* 12(9), 10307-10316.

Lu, Y., Fan, D., Shen, Z., Zhang, H., Xu, H., & Yang, X. (2022). Design and performance boost of a MOF-functionalized-wood solar evaporator through tuning the hydrogen-bonding interactions. *Nano Energy,* 95, 107016.

Lu, Y., Fan, D., Wang, Y., Xu, H., Lu, C., & Yang, X. (2021). Surface Patterning of Two-Dimensional Nanostructure-Embedded Photothermal Hydrogels for High-Yield Solar Steam Generation. *ACS Nano,* 15(6), 10366-10376.

Mathioulakis, E., Belessiotis, V., & Delyannis, E. (2007). Desalination by using alternative energy: Review and state-of-the-art. *Desalination,* 203(1), 346-365.

Meng, S., Zha, X.-J., Wu, C., Zhao, X., Yang, M.-B., & Yang, W. (2021). Interfacial Radiation-Absorbing Hydrogel Film for Efficient Thermal Utilization on Solar Evaporator Surfaces. *Nano Letters,* 21(24), 10516-10524.

Nagy, P. I., III, W. J. D., & Nicholas, J. B. (1989). Investigations on the convergence rate of the thermodynamic and structural parameters from Monte Carlo simulations of aqueous solutions of methanol and methylamine. *The Journal of Chemical Physics,* 91(6), 3707-3715.

Pauling, L. (1932). The nature of the chemical bond. Iv. The energy of single bonds and the relative electronegativity of atoms. *Journal of the American Chemical Society,* 54(9), 3570-3582.

Rablen, P. R., Lockman, J. W., & Jorgensen, W. L. (1998). Ab Initio Study of Hydrogen-Bonded Complexes of Small Organic Molecules with Water. *The Journal of Physical Chemistry A,* 102(21), 3782-3797.

Rizzo, R. C., & Jorgensen, W. L. (1999). OPLS All-Atom Model for Amines: Resolution of the Amine Hydration Problem. *Journal of the American Chemical Society,* 121(20), 4827-4836.

Shahzad, M. W., Burhan, M., Ang, L., & Ng, K. C. (2017). Energy-water-environment nexus underpinning future desalination sustainability. *Desalination,* 413, 52-64.

Shannon, M. A., Bohn, P. W., Elimelech, M., Georgiadis, J. G., Mariñas, B. J., & Mayes, A. M. (2008). Science and technology for water purification in the coming decades. *Nature,* 452(7185), 301-310.

Shao, B., Wang, Y., Wu, X., Lu, Y., Yang, X., Chen, G. Y., . . . Xu, H. (2020). Stackable nickel–cobalt@polydopamine nanosheet based photothermal sponges for highly efficient solar steam generation. *Journal of Materials Chemistry A,* 8(23), 11665-11673.

Simončič, M., & Urbic, T. (2018). Hydrogen bonding between hydrides of the upper-right part of the periodic table. *Chemical Physics,* 507, 34-43.

Storer, D. P., Phelps, J. L., Wu, X., Owens, G., Khan, N. I., & Xu, H. (2020). Graphene and Rice-Straw-Fiber-Based 3D Photothermal Aerogels for Highly Efficient Solar Evaporation. *ACS Applied Materials & Interfaces,* 12(13), 15279-15287.

Tao, P., Ni, G., Song, C., Shang, W., Wu, J., Zhu, J., . . . Deng, T. (2018). Solar-driven interfacial evaporation. *Nature Energy,* 3(12), 1031-1041.

Tarazona-Romero, B. E., Campos-Celador, A., & Maldonado-Muñoz, Y. A. (2022). Can solar desalination be small and beautiful? A critical review of existing technology under the appropriate technology paradigm. *Energy Research & Social Science,* 88, 102510.

Trivedi, T. J., Rao, K. S., & Kumar, A. (2014). Facile preparation of agarose–chitosan hybrid materials and nanocomposite ionogels using an ionic liquid via dissolution, regeneration and sol–gel transition. *Green Chemistry,* 16(1), 320-330.

Vardar, E., Vert, M., Coudane, J., Hasirci, V., & Hasirci, N. (2012). Porous Agarose-Based Semi-IPN Hydrogels: Characterization and Cell Affinity Studies. *Journal of Biomaterials Science, Polymer Edition,* 23(18), 2273-2286.

Wang, P. (2018). Emerging investigator series: the rise of nano-enabled photothermal materials for water evaporation and clean water production by sunlight. *Environmental Science: Nano,* 5(5), 1078-1089.

Wang, Y., Wu, X., Gao, T., Lu, Y., Yang, X., Chen, G. Y., . . . Xu, H. (2021). Same materials, bigger output: A reversibly transformable 2D–3D photothermal evaporator for highly efficient solar steam generation. *Nano Energy,* 79, 105477.

Wang, Z., Horseman, T., Straub, A. P., Yip, N. Y., Li, D., Elimelech, M., & Lin, S. (2019). Pathways and challenges for efficient solar-thermal desalination. *Science Advances,* 5(7), eaax0763.

Wang, F., Wei, D., Li, Y., Chen, T., Mu, P., Sun, H., . . . Li, A. (2019). Chitosan/reduced graphene oxide-modified spacer fabric as a salt-resistant solar absorber for efficient solar steam generation. *Journal of Materials Chemistry A,* 7(31), 18311-18317.

Wang, W., Shi, Y., Zhang, C., Li, R., Wu, M., Zhuo, S., . . . Wang, P. (2021). Solar Seawater Distillation by Flexible and Fully Passive Multistage Membrane Distillation. *Nano Letters,* 21(12), 5068-5074.

Wang, X., Zhang, L., Zheng, D., Xu, X., Bai, B., & Du, M. (2023). A polyelectrolyte hydrogel coated loofah sponge evaporator based on Donnan effect for highly efficient solar-driven desalination. *Chemical Engineering Journal,* 462, 142265.

Xu, Y., Xu, J., Zhang, J., Li, X., Fu, B., Song, C., . . . Deng, T. (2022). All-in-one polymer sponge composite 3D evaporators for simultaneous high-flux solar-thermal desalination and electricity generation. *Nano Energy,* 93, 106882.

Yu, F., Chen, Z., Guo, Z., Irshad, M. S., Yu, L., Qian, J., . . . Wang, X. (2020). Molybdenum Carbide/Carbon-Based Chitosan Hydrogel as an Effective Solar Water Evaporation Accelerator. *ACS Sustainable Chemistry & Engineering,* 8(18), 7139-7149.

Yu, Z., Gu, R., Tian, Y., Xie, P., Jin, B., & Cheng, S. (2022). Enhanced Interfacial Solar Evaporation through Formation of Micro-Meniscuses and Microdroplets to Reduce Evaporation Enthalpy. *Advanced Functional Materials,* 32(17), 2108586.

Yu, Z., Gu, R., Zhang, Y., Guo, S., Cheng, S., & Tan, S. C. (2022). High-flux flowing interfacial water evaporation under multiple heating sources enabled by a biohybrid hydrogel. *Nano Energy,* 98, 107287.

Zhang, Y., Ravi, S. K., Yang, L., Vaghasiya, J. V., Suresh, L., Tan, I., & Tan, S. C. (2019). Portable Trilayer Photothermal Structure for Hybrid Energy Harvesting and Synergic Water Purification. *ACS Applied Materials & Interfaces,* 11(42), 38674-38682.

526 Zhang, Y., Xiong, T., Nandakumar, D. K., & Tan, S. C. (2020). Structure Architecting for Salt-
527 Rejecting Solar Interfacial Desalination to Achieve High-Performance Evaporation With
528 In Situ Energy Generation. *Advanced Science,* 7(9), 1903478.

529 Zhang, Y., Xiong, T., Suresh, L., Qu, H., Zhang, X., Zhang, Q., . . . Tan, S. C. (2020). Guaranteeing
530 Complete Salt Rejection by Channeling Saline Water through Fluidic Photothermal
531 Structure toward Synergistic Zero Energy Clean Water Production and in Situ Energy
532 Generation. *ACS Energy Letters,* 5(11), 3397-3404.

533 Zhang, B., Wong, P. W., & An, A. K. (2022). Photothermally enabled MXene hydrogel
534 membrane with integrated solar-driven evaporation and photodegradation for efficient
535 water purification. *Chemical Engineering Journal,* 430, 133054.

536 Zhuang, P., Li, D., Xu, N., Yu, X., & Zhou, L. (2021). Stable Self-Floating Reduced Graphene
537 Oxide Hydrogel Membrane for High Rate of Solar Vapor Evaporation under 1 sun.
538 *Global Challenges,* 5(1), 2000053.

539 Zhao, F., Guo, Y., Zhou, X., Shi, W., & Yu, G. (2020). Materials for solar-powered water
540 evaporation. *Nature Reviews Materials*.

541 Zhou, X., Guo, Y., Zhao, F., & Yu, G. (2019). Hydrogels as an Emerging Material Platform for
542 Solar Water Purification. *Accounts of Chemical Research,* 52(11), 3244-3253.

543 Zhou, X., Zhao, F., Guo, Y., Rosenberger, B., & Yu, G. (2019). Architecting highly hydratable
544 polymer networks to tune the water state for solar water purification. *Science Advances,*
545 5(6), eaaw5484.

546